

REFERENCES AND NOTES

1. K. Wyrki, *Deep-Sea Res.* **8**, 39 (1961); W. H. Munk, *ibid.* **13**, 207 (1966); A. E. Gargett, *J. Mar. Res.* **42**, 359 (1984).
2. H. Stommel and A. B. Arons, *Deep-Sea Res.* **6**, 140 (1960).
3. N. G. Hogg, P. Biscaye, W. Gardner, W. J. Schmitz, *J. Mar. Res. (Suppl.)* **40**, 231 (1982).
4. J. A. Whitehead and L. V. Worthington, *J. Geophys. Res.* **87**, 7903 (1982); P. M. Saunders, *J. Phys. Oceanogr.* **17**, 631 (1987); E. D. Barton and A. E. Hill, *Deep-Sea Res.* **36**, 1121 (1989); D. Roemmich, S. Hautala, D. Rudnick, *J. Geophys. Res.* **101**, 14039 (1996). Characteristic of these studies, a heat flux divergence is found, associated with bottom water flowing horizontally into a basin at a colder average temperature than it leaves by upwelling across isotherms. This divergence is presumed to be balanced by downward turbulent diffusion, with the requisite heat flux commonly expressed as a vertical diffusivity (K) multiplied by the mean vertical temperature gradient averaged horizontally over the basin.
5. M. C. Gregg, *J. Geophys. Res.* **94**, 9686 (1989); K. L. Polzin *et al.* *J. Phys. Oceanogr.* **25**, 306 (1995).
6. J. R. Ledwell, A. J. Watson, C. S. Law, *Nature* **364**, 701 (1993).
7. M. C. Gregg, *J. Phys. Oceanogr.* **7**, 436 (1977); J. N. Moum and T. R. Osborn, *ibid.* **16**, 1250 (1986); E. Kunze and T. B. Sanford, *ibid.* **26**, 2286 (1996).
8. J. M. Toole *et al.* *Science* **264**, 1120 (1994).
9. J. M. Toole, R. W. Schmitt, K. L. Polzin, E. Kunze, *J. Geophys. Res.* **102**, 947 (1997).
10. R. W. Schmitt *et al.* *J. Atmos. Ocean. Technol.* **5**, 484 (1988).
11. T. R. Osborn and C. S. Cox, *Geophys. Fluid Dyn.* **3**, 321 (1972); T. R. Osborn, *J. Phys. Oceanogr.* **10**, 83 (1980).
12. C. S. Law *et al.* *Mar. Chem.* **48**, 57 (1994).
13. X. Durrieu De Madron and G. Weatherly, *J. Mar. Res.* **52**, 583 (1994).
14. The tracer was injected into the ocean in a series of streaks by use of a tethered system that was towed behind the research vessel while being positioned vertically to remain within a few meters of a target density surface. Subsequent spread of the tracer was documented with water sample analysis conducted at sea with a gas chromatograph equipped with an electron capture detector (12).
15. J. R. Ledwell and A. Bratkovich, *J. Geophys. Res.* **100**, 20681 (1995).
16. T. H. Bell, *J. Fluid Mech.* **67**, 705 (1975); *J. Geophys. Res.* **80**, 320 (1975); P. G. Baines, *Deep-Sea Res.* **29**, 307 (1982); B. Sjöberg and A. Stigebrandt, *ibid.* **39**, 269 (1992); S. A. Thorpe, *Proc. R. Soc. London Ser. A* **439**, 115 (1995).
17. Shear is the vertical variation of the horizontal velocity, and strain is the vertical gradient of vertical displacements, the latter inferred from variations in the separation between isopycnals.
18. O. M. Phillips, *The Dynamics of the Upper Ocean* (Cambridge Univ. Press, New York, ed. 2, 1977); C. C. Eriksen, *J. Geophys. Res.* **87**, 525 (1982); C. Garrett and D. Gilbert, in *Small-Scale Turbulence and Mixing in the Ocean, Proceedings of the 19th International Liege Colloquium on Ocean Hydrodynamics*, Liege, Belgium, 4 to 8 May 1987, J. C. J. Nihoul and B. M. Jamart, Eds. (Elsevier, New York, 1988), pp. 405–424.
19. F. S. Hotchkiss and C. Wunsch, *Deep-Sea Res.* **29**, 415 (1982).
20. C. Garrett and W. H. Munk, *J. Geophys. Res.* **80**, 291 (1975); J. L. Cairns and G. O. Williams, *ibid.* **81**, 1943 (1976).
21. Our estimate of the turbulent heat flux may be biased low for several reasons. First, more than 45% of the Brazil Basin might be categorized as "rough." The areal fractions assigned in Table 1 are based on our quasi-zonal sections. This breakdown does not, for example, include contributions to the rough-bottom category from the northern and southern boundaries of the Brazil Basin. Second, we most likely under-sampled the mixing on the 0.8°C isotherm where it lies close to the bottom over rough bathymetry. Many of our HRP stations in the eastern Brazil Basin were atop ridge spurs and consequently did not sample temperatures this low. A reanalysis of the heat budget of Hogg *et al.* at somewhat warmer bounding temperature for which we have more microstructure observations could address this. Third, there may be regional variation in the intensity of the mixing above rough bathymetry due to changes in the small-scale bottom roughness, near-bottom currents, and stratification, all of which affect the generation of internal waves.
22. K. L. Polzin *et al.* *Nature* **380**, 54 (1996).
23. σ_4 is the potential density referenced to 4000 dbar.
24. Including the flow across the Santos Plateau and Hunter Channel, K. G. Speer and W. Zenk [*J. Phys. Oceanogr.* **23**, 2667 (1993)] obtained a somewhat larger transport of about $5 \times 10^6 \text{ m}^3 \text{ s}^{-1}$.
25. H. Mercier and K. Speer, in preparation.
26. M. Hall, personal communication.
27. The diapycnal velocity w^* was estimated as $\sim 0.25 \text{ N}^{-2} \Delta \rho / \Delta z$ over a 100-m interval about the 0.8°C potential isotherm. The neglected terms in this equation (set in a coordinate system aligned with the density field) associated with nonlinearities in the seawater equation of state that cause densification of water on mixing [T. McDougall, in *Proceedings of Hawaiian Winter Workshop*, SOEST Special Publication, 13 to 19 January 1991 (Univ. of Hawaii at Manoa, 1991), pp. 355–386] only exacerbate the problem with the mass budget closure.
28. Equivalently, in the vertical, our estimates of ($K \partial_z \rho$) peak about the crests of the MAR spurs and decrease with still greater depth within the canyons.
29. With a flat bottom and uniform stratification, the flow would be zonal. However, basin-scale bottom-depth variations [Speer and Zenk (24)] and eddy-driven horizontal recirculations extending from the western boundary [M. A. Spall, *J. Mar. Res.* **52**, 1051 (1994)] may strongly distort this interior circulation from simple zonal flow.
30. C. Wunsch, *Deep-Sea Res.* **17**, 293 (1970); L. Thompson and G. C. Johnson, *ibid.* **43**, 193 (1996).
31. We thank E. Montgomery, D. Wellwood, T. Donoghue, B. Guest, T. Bolmer, S. Sutherland, and L. St. Laurent for support of our field program and data analysis, and the officers and crew of the R/V *Seward Johnson*. Supported by the NSF Division of Ocean Sciences. The HRP was developed with support from the Department of Defense and the Office of Naval Research.

16 December 1996; accepted 10 February 1997

The Atmospheric Aerosol-Forming Potential of Whole Gasoline Vapor

J. R. Odum, T. P. W. Jungkamp, R. J. Griffin, R. C. Flagan, J. H. Seinfeld*

A series of sunlight-irradiated, smog-chamber experiments confirmed that the atmospheric organic aerosol formation potential of whole gasoline vapor can be accounted for solely in terms of the aromatic fraction of the fuel. The total amount of secondary organic aerosol produced from the atmospheric oxidation of whole gasoline vapor can be represented as the sum of the contributions of the individual aromatic molecular constituents of the fuel. The urban atmospheric, anthropogenic hydrocarbon profile is approximated well by evaporated whole gasoline, and thus these results suggest that it is possible to model atmospheric secondary organic aerosol formation.

Several recent epidemiologic studies have consistently reported increased daily mortality associated with exposure to fine particulate air pollution (1, 2). An important contribution to the atmospheric fine particulate burden, especially during severe urban smog episodes, is secondary organic aerosol (SOA) (3). Like ozone (O_3), SOA is formed from the atmospheric oxidation of organic compounds. Whereas the oxidation of most hydrocarbons contributes to O_3 formation, SOA is generally formed only from the oxidation of hydrocarbon molecules containing seven or more carbon atoms (4). To form SOA, oxidation products must have vapor pressures that are sufficiently low to enable them to partition into the particulate phase.

In an effort to achieve urban and regional

O_3 abatement through the reduction of mass emissions of nonmethane hydrocarbons, the 1990 amendments to the U.S. Clean Air Act mandate the use of reformulated gasoline in motor vehicles. Several recent studies have suggested that a more effective approach to controlling urban O_3 associated with emissions from gasoline usage is to target the emissions of specific fuel components, rather than total nonmethane hydrocarbons, because of the extreme differences in the O_3 -forming potential of the hundreds of individual compounds that constitute gasoline (5). Considering the common link between urban O_3 formation and SOA formation, this approach may also be an effective way to control SOA formation associated with emissions from gasoline usage.

Organic aerosol formation potentials depend on two factors: reactivity of the parent compound and volatility of the product species. The reactivity of the parent species can be directly measured by reaction rate constants. However, because atmospheric chemical reaction pathways for large hydrocarbon molecules are complex and the re-

J. R. Odum and T. P. W. Jungkamp, Department of Environmental Engineering Science, California Institute of Technology, Pasadena, CA 91125, USA.
R. J. Griffin, R. C. Flagan, J. H. Seinfeld, Department of Chemical Engineering, California Institute of Technology, Pasadena, CA 91125, USA.

*To whom correspondence should be addressed.

sulting oxidation products are both numerous and difficult to quantify analytically, a more indirect measure of product volatility, the SOA yield Y , has been used. Traditionally, Y has been defined as the fraction of a reactive organic gas (ROG) that is converted to aerosol by means of atmospheric oxidation processes: $Y = \Delta M_o / \Delta ROG$, that is, the total mass concentration of organic aerosol, ΔM_o , produced for a given amount of ROG reacted, ΔROG . Yield data have been obtained for dozens of ROGs in controlled smog chamber studies (6–8).

The mixture of hydrocarbons that compose gasoline is representative of the atmospheric distribution of anthropogenic hydrocarbons in an urban airshed in terms of both complexity and composition (9), and therefore, determining the atmospheric aerosol formation potential of whole gasoline vapor is of significant interest. In general, gasoline contains four classes of reactive organics—oxygenates, alkanes, alkenes, and aromatics—which vary widely in their atmospheric reactivity and in the volatility of their atmospheric oxidation products. Our hypothesis is that the atmospheric aerosol-forming potential of whole gasoline vapor can be quantitatively accounted for in terms of the aromatic content of the fuel.

The outdoor smog chamber system used in this study has been described in detail previously (10). It consists of a 60-m³ sealed, collapsible polytetrafluoroethylene (Teflon) bag. Experiments are performed by (i) injecting into the bag (filled with humidified clean air) appropriate concentrations of seed aerosol [(NH₄)₂SO₄, about 5,000 to 10,000 particles per cubic centimeter, an initial aerosol volume of about 5 to 10 μm³ per cubic centimeter of air], a photochemical initiator [propene, about 150 to 300 parts per billion (ppb)], NO and NO₂, and the single hydrocarbon or hydrocarbon mixture of choice and then (ii) allowing the mixture to react under sunlight for 6 to 8 hours (11). During the course of the experiment, the concentration of each ROG species is either measured with the use of gas chromatography or is calculated on the basis of relative rates of reaction, in order to determine ΔROG . Particle number and size are measured continuously throughout the experiment by scanning electrical mobility spectrometers to determine ΔM_o (7, 12).

Because the oxidation products responsible for forming SOA are semivolatile and partition themselves between the gas and absorbing organic aerosol phases (10, 13), SOA yields for individual ROGs (Y) are a function of M_o . This dependence is represented by (10)

$$Y = M_o \sum_i \left(\frac{\alpha_i K_{om,i}}{1 + K_{om,i} M_o} \right) \quad (1)$$

where α_i and $K_{om,i}$ are the mass-based stoichiometric coefficient and absorption equilibrium partitioning coefficient of product i , respectively (14). Yield data for individual hydrocarbons can be fit well using Eq. 1 assuming a two-product model (that is, by choosing appropriate values for α_1 , α_2 , $K_{om,1}$, and $K_{om,2}$) (10). Organic aerosol yields were measured as a function of ΔM_o for 17 aromatic species that represent the predominant mass fraction of aromatics present in gasoline (Fig. 1). Most of the data can be fit with only two curves. Curve 1 corresponds to propylbenzene and to those species having one or fewer methyl substituents plus one or fewer ethyl substituents, and curve 2 fits species that contain two or more methyl substituents. Curves 3 and 4 fit the only diethylbenzene and methyl-*n*-propylbenzene species that were studied. There is little variation of the yield for different isomers. For example, *o*-, *m*-, and *p*-xylene all exhibit yields that are described by the same curve. It is likely that

parent species that are sufficiently similar in nature generate, upon photooxidation, semivolatile products that have similar gas-aerosol partitioning behavior.

From yield curves for individual parent hydrocarbons, like those shown in Fig. 1, one can account for the aerosol that is formed from the oxidation of a mixture of two species as the sum of the yields of the individual parent species present in the mixture (10). To ensure that the aerosol formed in a more complex mixture could be accounted for in such a manner, we performed an experiment in which a mixture of five different aromatic species (toluene, *m*-xylene, *m*-ethyltoluene, propylbenzene, and 1,2,4-trimethylbenzene) was photooxidized. The total organic aerosol concentration produced in the chamber was 28 μg m⁻³. Using the curves from Fig. 1, an appropriate yield value (Y_i) for each of the five aromatics, corresponding to a total organic aerosol mass concentration $\Delta M_o = 28 \mu\text{g m}^{-3}$, is obtained, and each value is multiplied by the respective reacted ROG con-

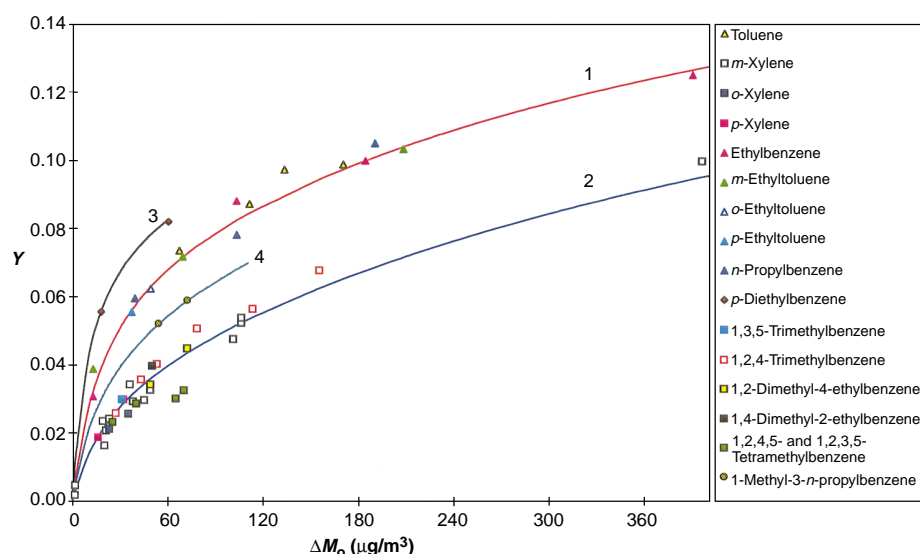


Fig. 1. Secondary organic aerosol yield as a function of total organic aerosol mass concentration (ΔM_o) for 17 individual aromatic species. Each point represents an individual experiment. Curves were fit to the data using a two-product model in conjunction with Eq. 1 by minimizing the weighted squared residuals. Curve 1 is fit with values 0.071, 0.053, 0.138, and 0.0019 for α_1 , $K_{om,1}$, α_2 , and $K_{om,2}$, respectively. The corresponding values are 0.038, 0.042, 0.167, and 0.0014 for curve 2; 0.083, 0.093, 0.22, and 0.0010 for curve 3; and 0.05, 0.054, 0.136, and 0.0023 for curve 4.

Table 1. Estimation of the contributions by individual species to the SOA formed from the photooxidation of a five-hydrocarbon mixture. Values of yield Y are taken from the curves shown in Fig. 1 at a value of $\Delta M_o = 28 \mu\text{g m}^{-3}$.

Species	Initial ROG ($\mu\text{g m}^{-3}$)	ΔROG ($\mu\text{g m}^{-3}$)	Y	$\Delta ROG \times Y$ ($\mu\text{g m}^{-3}$)
Toluene	663	265	0.049	13
<i>m</i> -Xylene	330	284	0.027	7.6
<i>m</i> -Ethyltoluene	105	89	0.049	4.4
<i>n</i> -Propylbenzene	40	16	0.049	0.8
1,2,4-Trimethylbenzene	162	147	0.027	3.9
Total				29.7

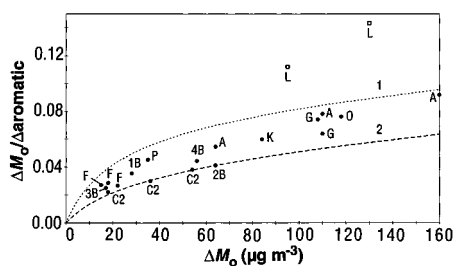


Fig. 2. Plot of $\Delta M_o/\Delta_{\text{aromatic}}$ as a function of ΔM_o for 12 different AQIRP gasolines (Table 2). Curves 1 and 2 are taken from Fig. 1. $\Delta M_o/\Delta_{\text{aromatic}}$ is equivalent to the SOA yield if Δ_{aromatic} is equal to Δ_{ROG} . Each point represents an individual experiment. Changes in ΔM_o for an individual fuel were obtained by varying fuel initial concentrations.

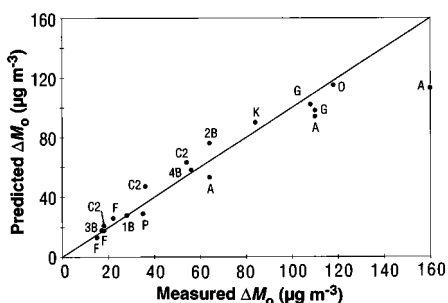


Fig. 3. Comparison between observed total SOA concentrations produced from the oxidation of whole gasoline vapor and total SOA concentrations predicted to be formed solely from the fuel's aromatic components.

centration (Δ_{ROG_i}) to produce an estimate of the amount of SOA attributed to each of the five species. Summing these values yields a total of $29.7 \mu\text{g m}^{-3}$, which is very close to the observed value of $28 \mu\text{g m}^{-3}$ (Table 1). Thus, by using SOA yields for the individual ROGs in conjunction with Eq. 1, one can account for the aerosol that is produced from the oxidation of the mixture.

We performed 20 smog chamber experiments with 12 different reformulated gasolines obtained from the Auto/Oil Air Quality Improvement Research Program (AQIRP) (Table 2) (15). Molecular speciation of the AQIRP fuels was used to calculate the reacted amount of each ROG (Δ_{ROG_i}) in the fuel mixture (16). We accomplished this procedure by quantifying the initial concentration of six to eight calibrated species present in each fuel using gas chromatography. Knowing the initial concentrations of these species, on the basis of the relative mass fractions of all the components in the fuel, we could calculate the initial concentration of every other species present. During the course of each experiment, the concentration time profiles of each of the calibrated species were measured and used along with their hydrox-

Table 2. Properties of AQIRP reformulated gasolines. MTBE = the fuel additive methyl tertiary butyl ether; the fuel identification code is derived from A (a) = high (low) aromatics, M (m) = high (low) MTBE, O (o) = high (low) olefins, T (t) = high (low) T_{90} ; RMH = medium and heavy reformat cut (predominantly C_9 and C_{10} aromatics), and AH = heavy alkylate cut (heavy paraffins).

Fuel code	AQIRP phase	Fuel ID	Aromatics (vol %)	MTBE (vol %)	Olefins (vol %)	T_{90} ($^{\circ}\text{C}$)
A	I	Industry average	32.0	0.0	9.2	166
F	I	amot	20.0	0.0	3.2	137
G	I	AmOt	44.3	0.0	17.4	141
K	I	Amot	45.7	0.0	4.9	146
L	I	AmOT	47.8	0.0	17.7	181
O	I	AMOT	46.7	14.6	19.3	139
P	I	amOt	20.3	0.0	18.3	140
C2	II	California phase II	25.4	11.2	4.1	145
1B	II	Matrix B base	25.3	11.2	15.0	131
2B	II	Base + RMH	35.1	10.4	11.2	157
3B	II	Base + AH	22.1	10.4	13.3	148
4B	II	Base + AH + RMH	32.2	10.2	10.7	168

yl radical (OH) rate constants to determine the concentration time profile of OH in the chamber (17). Typical OH concentrations were 10^6 molecules per cubic centimeter. This information, together with measured O_3 concentrations and the OH and O_3 rate constants for all other species, allowed us to determine the reacted amount of each species present in the fuel mixture during the course of an experiment.

The results of these experiments strongly support the hypothesis that aromatics play the predominant role in SOA formation associated with atmospheric oxidation of unburned gasoline. Plotting the ratio of the total SOA concentration produced from a given fuel to the reacted concentration of a fuel's aromatic constituents ($\Delta M_o/\Delta_{\text{aromatic}}$) versus ΔM_o (18) (Fig. 2), we see that points for all fuels other than RF-L fall within the range specified by the yield curves that describe the majority of SOA yields from the individual aromatic studies (curves 1 and 2 from Fig. 1) (19). If significant amounts of the SOA that was produced originated from species other than the aromatics, then most points would lie above the envelope specified by these two curves.

Using the curves for the 17 species shown in Fig. 1, and assuming that all isomers of a given compound behave similarly, we obtained yield curves for 19 of the 26 aromatics speciated in Phase I of the AQIRP study. These 19 species represented, on average, 96% of Δ_{aromatic} for all fuels other than RF-A and RF-L. Of the 57 speciated aromatic compounds for the AQIRP Phase II fuels, yield curves were available for 28, representing, on average, 95% of Δ_{aromatic} . Obtaining a yield value, corresponding to the amount of SOA formed in an individual experiment, for an individual aromatic (Y_i) and multiplying that value by the reacted amount of the respective aromatic (Δ_{ROG_i}) produces an

estimate of the amount of SOA attributable to that given aromatic species. Summing these values for all aromatics gives a quantitative estimate of the amount of SOA ($\Delta M_o = \sum_i \Delta_{\text{ROG}_i} Y_i$) that was produced by the aromatic fraction of each fuel (Fig. 3). These results quantitatively support the hypothesis that aromatic content controls a fuel's SOA formation potential. The average ratio of the SOA concentration predicted to be formed from a fuel's aromatic constituents to the observed SOA concentration for all fuels, excluding RF-L, is $1.00 \pm 0.16 (1\sigma)$. Thus, it is evident that aromatics dominate the process of SOA formation associated with the atmospheric oxidation of whole gasoline vapor. Given the chemical complexity of whole gasoline, the results of this study suggest that SOA formation in an urban airshed can be modeled using yield data such as those presented here.

REFERENCES AND NOTES

- J. Schwartz, D. W. Dockery, L. M. Neas, *J. Air Waste Manage. Assoc.* **46**, 927 (1996); D. S. Shprentz, *Breath Taking: Premature Mortality Due to Particulate Air Pollution in 239 American Cities* (National Resources Defense Council, New York, 1996); C. A. Pope III, D. V. Bates, M. E. Raizenne, *Environ. Health Perspect.* **103**, 472 (1995).
- Fine particulate matter, also known as $\text{PM}_{2.5}$ (that is, particles of diameter less than $2.5 \mu\text{m}$), is the respirable fraction of atmospheric particulate matter.
- B. J. Turpin and J. J. Huntzicker, *Atmos. Environ. A* **25**, 207 (1991); _____, S. M. Larson, G. R. Cass, *Environ. Sci. Technol.* **25**, 1788 (1991).
- D. Grosjean, *Atmos. Environ. A* **26**, 953 (1992); _____ and J. H. Seinfeld, *Atmos. Environ.* **23**, 1733 (1989).
- F. M. Bowman and J. H. Seinfeld, *Prog. Energy Combust. Sci.* **21**, 387 (1995); A. Russell et al., *Science* **269**, 491 (1995); J. G. Calvert, J. B. Heywood, R. F. Sawyer, J. H. Seinfeld, *ibid.* **261**, 37 (1993); S. K. Hoekman, *Environ. Sci. Technol.* **26**, 1206 (1992).
- S. N. Pandis et al., *Atmos. Environ. A* **25**, 997 (1991).
- S. C. Wang et al., *ibid.* **26**, 403 (1992).
- S. Hatakeyama, K. Izumi, T. Fukuyama, H. Akimoto, N. Washida, *J. Geophys. Res.* **96**, 947 (1991); K. Izumi and T. Fukuyama, *Atmos. Environ. A* **24**, 1433 (1990); J. E. Stern, R. C. Flagan, D. Grosjean, J. H.

- Seinfeld, *Environ. Sci. Technol.* **21**, 1224 (1987); M. W. Gery, D. L. Fox, H. E. Jeffries, *Int. J. Chem. Kinet.* **17**, 931 (1985); J. A. Leone, R. C. Flagan, D. Grosjean, J. H. Seinfeld, *ibid.*, p. 177; D. Grosjean, in *Ozone and Other Photochemical Oxidants* (National Academy of Sciences, Washington, DC, 1977), chap. 3.
9. R. A. Harley, M. P. Hannigan, G. R. Cass, *Atmos. Environ. A* **26**, 2395 (1992).
10. J. R. Odum *et al.*, *Environ. Sci. Technol.* **30**, 2580 (1996).
11. Initial hydrocarbon concentrations ranged from 400 to 5000 $\mu\text{g m}^{-3}$ for the individual aromatic experiments and from 2700 to 7000 $\mu\text{g m}^{-3}$ for the gasoline experiments. Concentrations of NO_x ($\text{NO} + \text{NO}_2$) were selected so that HC/NO_x ratios typical of those in an urban environment (5 to 10 ppbC/ppb NO_x) were achieved. The ratio of NO/NO_2 was always set at 2.
12. Scanning electrical mobility spectrometers were used to obtain complete particle number and size distributions with a 1-min frequency. Time-dependent particle volume concentrations were calculated from these distributions. The time-dependent cumulative organic volume concentration was calculated by subtracting the volume concentration at time t (corrected for deposition) from the initial volume concentration. Total organic mass concentrations were calculated from the total cumulative organic volume concentration assuming the density of the condensed organic phase was 1 g cm^{-3} .
13. J. F. Pankow, *Atmos. Environ. A* **28**, 185 (1994).
14. Parameter K_{om} is an equilibrium constant describing the partitioning of semivolatile organics between the vapor phase and an absorbing organic condensed phase: $K_{\text{om}} = (F/M_o)/A$, where F and A are a semivolatile compound's concentration in the absorbing organic and vapor phases, respectively, and M_o is the concentration of the absorbing organic aerosol.
15. AQIRP was a cooperative program whose members included three domestic auto companies and 14 petroleum companies, the objective of which was to develop data on the potential improvements in vehicle emissions and air quality, primarily O_3 , from reformulated gasoline, various other alternative fuels, and developments in automotive technology. V. R. Burns *et al.*, *SAE Tech. Pap. 912320* (Society of Automotive Engineers, Warren, PA, 1991); A. M. Hochhauser *et al.*, *SAE Tech. Pap. 912322* (Society of Automotive Engineers, Warren, PA, 1991).
16. R. H. Paul and M. J. McNally, *SAE Tech. Pap. 902098* (Society of Automotive Engineers, Warren, PA, 1991); W. O. Siegl *et al.*, *SAE Tech. Pap. 930142* (Society of Automotive Engineers, Warren, PA, 1993).
17. Hydroxyl radical and O_3 rate constants were taken from review literature (20) and the National Institute of Standards and Technology (NIST) chemical kinetics database (21) or, when experimentally not known, were estimated with the structure reactivity relations (SARs) (22). The SAR expressions for alkanes and alkenes were used unchanged; we modified those for aromatics by deriving a new Hammett constant for metasubstituents (σ_m^+). We optimized σ_m^+ for the ring addition rate constant (k_{add}) of 15 alkyl-substituted aromatics. The expression derived for use within SAR was $\log_{10} k_{\text{add}} (\text{cm}^3 \text{ molecule}^{-1} \text{ s}^{-1}) = -11.89 - 1.82\sigma_m^+$, where $\sigma_m^+ = \sigma_m^+$ and σ_m^+, p , with $\sigma_m^+ = -0.190$ for all *meta*-alkyl substituents and Hammett constants for ortho and para substituents (σ_{ortho} , σ_{para}) as used in (22). The quality of the fit for the overall OH rate constant estimates for aromatics was improved to 30% maximum error, compared to 110% using the parameters in (22).
18. The value of Δ_{aromatic} was calculated by summing the reacted amount of each aromatic species in a fuel for a given experiment. The ratio of $\Delta M_o/\Delta_{\text{aromatic}}$ is a measure of the SOA yield of a fuel in terms of its aromatic fraction only. For the individual aromatic experiments, $\Delta M_o/\Delta_{\text{aromatic}} = Y$.
19. For most fuels, 92 to 99% of the mass was speciated in AQIRP (16). Only 83% of the mass of fuel RF-L, which was the only high T_{90} AQIRP Phase I fuel used in this study, was speciated in AQIRP (23). Much of the remaining 17% of the mass of this fuel is most likely heavy aromatic species that contribute to the

SOA formed from the oxidation of this fuel. Because this 17% was not speciated, Δ_{aromatic} for this fuel is most likely underestimated, explaining why this fuel does not fall within the envelope as all other fuels specified by curves 1 and 2 (Fig. 2).

20. R. Atkinson, *J. Phys. Chem. Ref. Data Monogr.* **2** (1994).
21. NIST Chemical Kinetics Database ver. 6.01; W. G. Mallard, F. Westley, J. T. Herron, R. F. Hampson, NIST Standard Reference Data, Gaithersburg, MD (1994).
22. E. S. C. Kwok and R. Atkinson, *Atmos. Environ. A* **29**, 1685 (1995).
23. Temperature T_{90} is the distillation temperature at which 90% of the fuel evaporates. It relates to a fuel's heavy-end volatility: Fuels with high T_{90} contain a significant fraction of heavy components. In

Phase I of the AQIRP, only 143 compounds were speciated, and many of the heavy components (including aromatics) were not accounted for. In Phase II, 320 compounds were speciated, and many of the heavier aromatics were accounted for. Thus, more than 94% of the carbon, on average, was accounted for in all Phase II fuels (both high and low T_{90}).

24. We would like to acknowledge support by the U.S. Environmental Protection Agency Center on Airborne Organics, the National Science Foundation, the Deutsche Forschungsgemeinschaft, the Coordinating Research Council, and the Chevron Corporation. We would also like to thank S. Kent Hoekman for his helpful comments.

2 December 1996; accepted 5 February 1997

Metathesis of Alkanes Catalyzed by Silica-Supported Transition Metal Hydrides

Véronique Vidal, Albert Théolier, Jean Thivolle-Cazat, Jean-Marie Basset*

The silica-supported transition metal hydrides ($\equiv\text{Si-O-Si}\equiv$)($\equiv\text{Si-O}$)₂Ta-H and ($\equiv\text{Si-O}$)_xM-H (M, chromium or tungsten) catalyze the metathesis reaction of linear or branched alkanes into the next higher and lower alkanes at moderate temperature (25° to 200°C). With ($\equiv\text{Si-O-Si}\equiv$)($\equiv\text{Si-O}$)₂Ta-H, ethane was transformed at room temperature into an equimolar mixture of propane and methane. Higher and lower homologs were obtained from propane, butane, and pentane as well as from branched alkanes such as isobutane and isopentane. The mechanism of the step leading to carbon-carbon bond cleavage and formation likely involves a four-centered transition state between a tantalum-alkyl intermediate and a carbon-carbon σ -bond of a second molecule of alkane.

Paraffins, particularly methane and light alkanes, constitute an abundant yet low-value fossil feedstock. Light alkanes would be very valuable if they could be transformed into higher molecular weight hydrocarbons (1); this represents a continuing scientific challenge (2). Here, we report observations of a catalytic reaction that we designate "metathesis of alkanes" and which, to our knowledge, has not previously been reported (3). The metathesis reaction proceeds by both the cleavage and the formation of the C-C bonds of acyclic alkanes, which are transformed into a mixture of higher and lower homologs. It was observed in the presence of various silica-supported metal-hydride catalysts, particularly tantalum hydride (4), all prepared by the surface organometallic chemistry route (5, 6). Metathesis reactions of alkenes and alkynes, discovered a few decades ago, are now well documented and understood and are used in several industrial chemical processes. In contrast to the metathesis of alkenes (7) or alkynes (8), for which the cleavage of the molecule occurs selectively at the C=C or

C≡C bond, the metathesis of acyclic alkanes seems to involve, at least to some extent, the reaction of all C-C bonds. Thus, the reaction, even if it is selective in terms of the formation and cleavage of C-C bonds, is not restricted to the formation of the first higher and lower homologs but also can yield the next several higher and lower ones. The metathesis of acyclic olefins is hindered by thermodynamic limitations; such a reaction is close to thermoneutrality for most alkanes (9).

We recently reported that the reaction of Ta(-CH₂CMe₃)₃(=CHCMe₃) (Me, methyl) (10) with the surface hydroxyl groups of a dehydroxylated silica (11) leads to the formation of a mixture of two species: ($\equiv\text{Si-O}$)Ta(-CH₂CMe₃)₂(=CHCMe₃) (~65%) and ($\equiv\text{Si-O}$)₂Ta(-CH₂CMe₃) (=CHCMe₃) (~35%) (12). Treatment of these two surface complexes under hydrogen at 150°C overnight yields mainly a surface tantalum (III) monohydride, ($\equiv\text{Si-O-Si}\equiv$)($\equiv\text{Si-O}$)₂Ta-H ([Ta]_s-H), which has been fully characterized by infrared spectroscopy, extended x-ray absorption fine structure (EXAFS) analysis, microanalysis, and quantitative chemical reactions (4).

When [Ta]_s-H was contacted at room temperature with a cyclic alkane (4, 13), no catalytic reaction occurred. Only a C-H

Laboratoire de Chimie Organométallique de Surface, UMR CNRS-CPE 9986, 43 Boulevard du 11 Novembre 1918, 69616 Villeurbanne Cédex, France.

*To whom correspondence should be addressed.